PCCP

Check for updates

Molecular dynamics of the halloysite nanotubes

Danil A. Prishchenko, [ID] *[a] Evgeniy V. Zenkov,[a] Vladimir V. Mazurenko,[a] Rawil F. Fakhrullin, [ID] [b] Yuri M. Lvov[ac] and Vladimir G. Mazurenko[a]

We report large-scale and long-time molecular dynamics simulations demonstrating the transformation of a single kaolin alumosilicate sheet to a halloysite nanotube. The models we consider contain up to 5×10^5 atoms, which is two orders of magnitude larger than that used in previous theoretical works. It was found that the temperature plays a crucial role in the formation of the rolled geometry of the halloysite. For the models with periodic boundary conditions, we observe the tendency to form twin-tube structures, which is confirmed experimentally by atomic force microscopy imaging. The molecular dynamics calculations show that the rate of the rolling process is very sensitive to the choice of the winding axis and varies from 5 ns to 25 ns. The effects of the open boundary conditions and the initial form of the kaolin alumosilicate sheet are discussed. Our simulation results are consistent with experimental TEM and AFM halloysite tube imaging.

1 Introduction

Natural tubular halloysite clay has attracted great interest in materials development because it is one of the few inexpensive nanomaterials available in thousand of tons at low price.[1–3] It is a safe and biocompatible alumosilicate that may be applied in functional polymeric nanocomposites with anticorrosion, antiaging and flame-retardant properties, in advanced metal–ceramic mesoporous catalysts, in bio-scaffolds, and for sustained drug delivery. Halloysite tubes have internal/external diameters as *ca.* 15 and 50 nm (Fig. 1).[4] Mineralogists have discussed the origin of halloysite tube formation and advocated for the direct rolling of pre-formed kaolin sheets. Another opinion is that spiral epitaxial growth of multilayer tubes may also be responsible for the halloysite formation.[5–8] Halloysite tubes can be experimentally produced by time-extended sonication of kaolin clay in water with the addition of detergents, which lends credibility to the first explanation of the origin of halloysite.[9]

Despite the growing number of technological applications and investigations on the physical properties of halloysite with the chemical formula $Al_2Si_2O_5(OH)_4$, there is still no consistent theoretical description of the mechanisms of its rolling, and the formation of tubular halloysite still remains an issue. One of the popular scenarios is that the driving force of the rolling
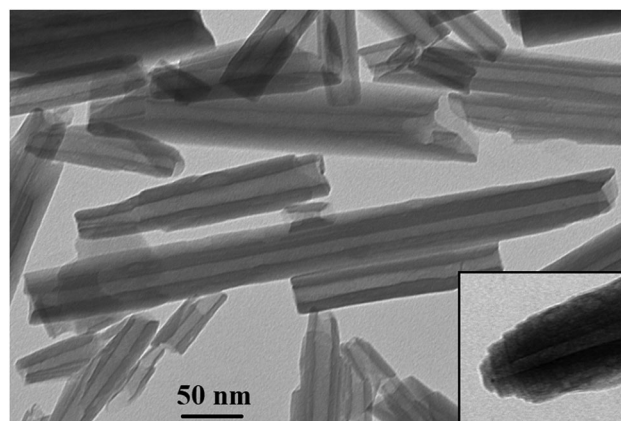

Fig. 1 Transmission electron microscopy image (Hitachi HD 2000 STEM, 100 kV) of halloysite nanotubes from Applied Minerals Inc, USA. Inset: The unbroken end of the tube indicating its roll-structure.

of an initially plate kaolinite specimen with Si–O tetrahedra on the outer side of the tube is related to geometric factors, *e.g.* the excess of the Si-tetrahedral sheet length over the length of Al-dioctahedral sheet (Fig. 2). Such a geometric model of spontaneous rolling of plate kaolinite samples provides only a qualitative understanding of the problem. On the other hand, microscopic models taking into account chemical composition and chemical bonding are needed to get insight into the nature of the rolling of kaolinite sheet and the influence of external conditions (temperature, pressure) on the geometry and energy of the halloysite.

Experimentally, the transformation of kaolinite to halloysite was observed in scanning tunnel microscopy studies.[6,10,11]

[a] *Theoretical Physics and Applied Mathematics Department, Ural Federal University, Mira Str. 19, Ekaterinburg, Russia. E-mail: clasius@yandex.ru*

[b] *Institute of Fundamental Medicine and Biology, Kazan Federal University, Kazan, Republic of Tatarstan, 420008, Russian Federation*

[c] *Institute for Micromanufacturing, Louisiana Tech University, Ruston, LA 71272, USA*
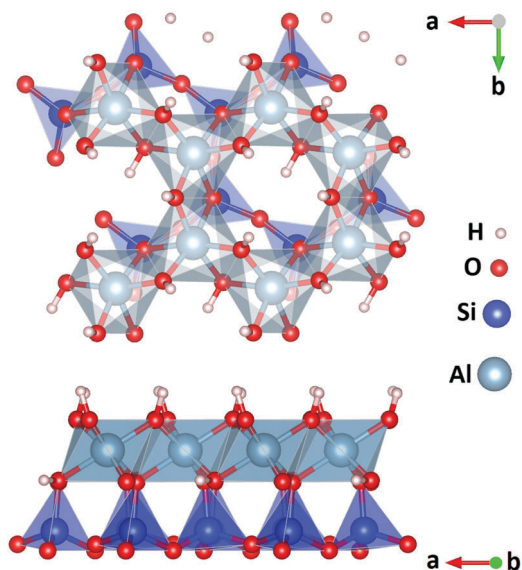
Fig. 2 Top (top panel) and side (bottom panel) views of a single kaolinite sheet. The images were created with the VESTA[17] program by using atomic positions optimized in DFT calculations.
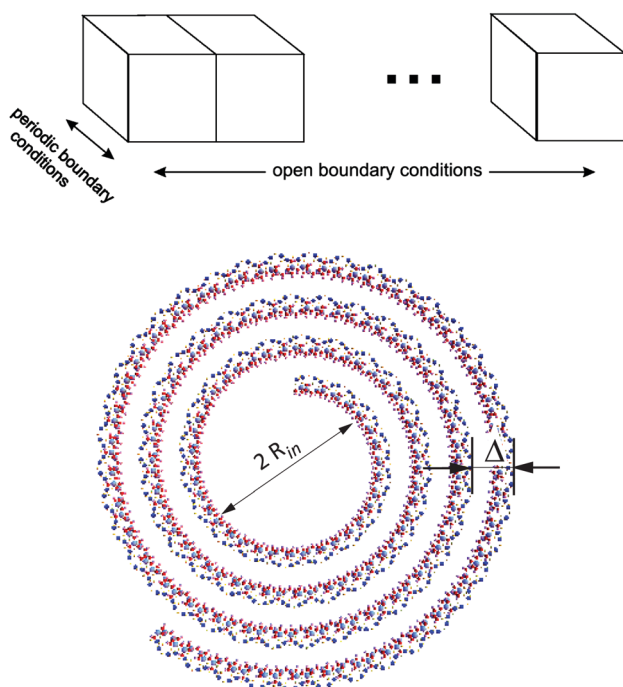

Fig. 3 Top: Schematic representation of the supercell used in this work for numerical simulations. Bottom: Example of the halloysite tube with the definition of interlayer distance, Δ, and inner radius, R_{in}.

Such experimental studies have revealed a principal role of hydration in the rolling of plate kaolinite. This process was also experimentally reproduced in the laboratory.[9] Moreover, there is a plethora of other experimental facts concerning the formation of the halloysite to be explained. First, there is the intricate atomic structure of the inner side of the halloysite tube (Fig. 4 in ref. 10, Fig. 13 in ref. 11, Fig. 9 in ref. 6). Second, there is variability of the

orientations of various tubular halloysite samples: while the winding axis is more commonly aligned in the crystalline b-direction, samples with orientations of the winding axes in the ab-plane are also known.[12–14]

From the theoretical side, previous computer simulations of halloysite were mainly focused on the electronic and structural properties of the simplified halloysite models, for instance, the single-walled[4] nanotube (which was not actually observed experimentally, because natural halloysite is always a multilayer tube[1–3]), spiral nanotube with overlapping arms[15] and two-slab[16] models. In these works, the authors mainly used the models with pre-defined forms and geometry that were further specified by means of a structural optimization. The main problem preventing the realistic description of halloysite is the extremely large size and multi-walled spiral structure of the individual nanotube. In this situation, the molecular dynamics approaches can give very important information concerning the chemical stability and evolution of the chemical bonding between halloysite and different molecular complexes or nanoparticles. For instance, the authors of ref. 16 reported on the dynamics of water adsorbed on kaolinite surfaces and confined in the halloysite interlayer. On the other hand, similar approaches can also be used for the simulation of the rolling process during the halloysite nanotube formation. However, this requires an accurate choice of the appropriate potential that should take into account the long-range Coulomb interactions and complex chemical composition of the halloysite.

Here, by using a combination of theoretical and experimental methods that are classical molecular dynamics (MD) simulations and atomic force microscopy (AFM), we study the formation of the halloysite nanotubes. The inter-atomic potential giving reliable results in the case of the kaolinite and two-slab model of halloysite[16] was adopted. This gives us an opportunity to trace the rolling process of the individual kaolinite sheet into different forms of halloysite nanotubes at finite temperatures. We observe a variety of tubular profiles with diameters ranging from 10 to 30 nm depending on the numerical scheme used for taking into account the Coulomb interaction. For the artificially rolled halloysites with an ideal cylindrical geometry, we revealed dependencies of the total energy of the system on the diameter and number of layers of the nanotube.

2 Experimental and theoretical methods

2.1 Atomic force microscopy (AFM) imaging

Atomic force microscopy images were collected using a Bruker Dimension FastScan microscope, operating in PeakForce Tapping mode.[18] For AFM imaging in air, the halloysite nanotubes were washed with ultrapure water (Simplicity Millipore), then placed directly onto dust-free Nexterion glass slides (Schott). AFM imaging in air was performed using ScanAsyst-Air probes (Bruker) (nominal length 115 µm, tip radius 2 nm, spring constant 0.4 N m^{-1}). The images were obtained at 512–1024 lines per scan at a scan rate of 0.8–0.9 Hz to secure the high imaging resolution and mechanical properties mapping. The images were collected in height sensor,

Young's modulus and adhesion channels. The raw AFM images were processed using Nanoscope Analysis v.1.7. software (Bruker).

2.2 Model and computational methods

To study the molecular dynamics of the halloysite slab, we used the LAMMPS[19] package, which allows us to calculate inter-atomic forces based on the type of the used potential. In this study, we used the ClayFF[20] inter-atomic potential, which can be represented as

$$E_{\text{total}} = E_{\text{Coulomb}} + E_{\text{vdW}} + E_{\text{bond}} + E_{\text{angle}}, \quad (1)$$

where

$$E_{\text{Coulomb}} = \frac{e^2}{4\pi\varepsilon_0} \sum_{i \neq j} \frac{q_i q_j}{r_{ij}}, \quad (2)$$

$$E_{\text{vdW}} = \sum_{i \neq j} D_{0,ij} \left[\left(\frac{R_{0,ij}}{r_{ij}} \right)^{12} - 2 \left(\frac{R_{0,ij}}{r_{ij}} \right)^{6} \right], \quad (3)$$

$$E_{\text{bond}} = \sum_{\text{bonds}} K_1 \left(r_{ij} - r_0 \right)^2, \quad (4)$$

$$E_{\text{angle}} = \sum_{\text{angles}} K_2 \left(\theta_{ijk} - \theta_0 \right)^2. \quad (5)$$

Here, r_{ij} and θ_{ijk} are distances and angles between different sites, respectively. D_0, R_0, K_1, K_2, r_0 and θ_0 are potential parameters, q is the charge and ε_0 is the electric constant. The first two terms are applied to every atomic pair, while the latter two affect only the O–H bonds and O–H–Al angles. In our study, we used the potential parameters taken from ref. 16 (Table 1), where the same type of inter-atomic potential was successfully used to study the MD of kaolinite.

We used the Ewald summation method with a real-space cut-off of 12 Å for small systems with numbers of atoms up to 3000. For larger systems, a Coulomb potential with an 8 Å cut-off radius was applied. We compare and discuss the results, obtained by both schemes, in Section 3.1.

MD simulations were performed using a canonical *NVT* ensemble with 0.5 fs timestep. A coupling constant of 0.5 ps was used for the interaction with the thermostat. We found that the stabilisation of the total energy for a given temperature requires up to 3 ns. Therefore, at least 10 ns molecular dynamics were always used, which also guarantees that the atomic structure arrives at equilibrium.

The unit cell used in molecular dynamics simulations has been prepared as follows. The primitive cell of kaolinite was taken from ref. 21. The translation vector in the *c* direction was artificially increased to introduce a vacuum of 20 Å between replicas. Then, we performed crystal structure optimization using the conjugated gradients algorithm as implemented in the plane-wave pseudopotential Vienna Ab Initio Simulation Package (VASP).[22,23] Projector augmented wave potentials have been used for this calculation. We make use of the Perdew, Burke, and Ernzerhof (PBE) generalized gradient approach (GGA) with a plane-wave cut-off energy equal to 400 eV. The *k*-mesh with ($6 \times 6 \times 1$) has been chosen for this simulation. The translation vectors of the unit cell were fixed such that only the ions were moved during these simulations. The unit cell parameters of the thus-obtained optimized structure are listed in Table 5.

3 Results

3.1 Ewald summation scheme

The main purpose of our study is to investigate the process of the transformation of halloysite from a single kaolinite sheet to the tubular form by using large-scale molecular dynamics models. In this section, we discuss the effects of long-ranged Coulomb interactions on the molecular dynamics of the kaolinite sheets. In the case of the three-dimensional periodic systems, the straightforward way to include those interactions is to apply the Ewald summation scheme. The problem is that this method requires significant computational resources even for small systems.[24] For large systems (with numbers of atoms more than 3000), one needs to use a more computationally efficient scheme. For example, in this study, we adopted a simple Coulomb cut-off potential. The main problem here is that such a simple potential does not take into account long-ranged contributions to the Coulomb interaction. We probe this potential *versus* the full Ewald calculation to understand the effect of neglecting long-ranged contributions to the Coulomb energy.

As the first step, we calculated the molecular dynamics of the 30 nm long kaolin alumosilicate sheet using the Ewald summation scheme, as shown in Fig. 4a. Then, we performed several MD runs with different halloysite sheet lengths and different cut-offs. We found that for a cut-off radius ranging between 7 and 9 Å, the sheet rolls such that the alumina side faces inside the tube, while for other cut-offs (up to 30 Å), halloysite rolls with the Al-side facing outward. Based on these results, we chose 8 Å as a cut-off radius. The main difference between the results obtained with the Ewald summation scheme and cut-off potential is that the inner radius of the nanotube is 3 times larger in the case of the cut-off potential (Fig. 4).

Table 1 Inter-atomic potential parameters taken from ref. 16, used in this work

Non-bond parameters				
Species	Symbol	Charge (e)	D_0 (kcal mol^{-1})	R_0 (Å)
Hydroxyl H	hh	0.425		
Hydroxyl O	oh	−0.950	0.1554	3.5532
Bridging O	ob	−1.050	0.1554	3.5532
Tetrahedral Si	st	2.100	1.8405×10^{-6}	3.7064
Octahedral Al	ao	1.575	1.3298×10^{-6}	4.7943

Bond parameters			
Species i	Species j	K_1 (kcal mol^{-1} Å^{-2})	r_0 (Å)
Oh	Hh	554.1349	1.0

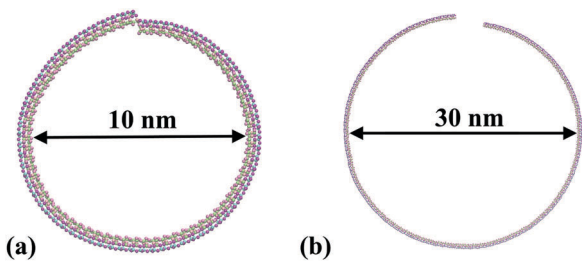| Angle parameters				
Species i	Species j	Species k	K_2 (kcal mol^{-1} rad^{-2})	θ_0 (deg)
Oh	Hh	Ao	30.0	109.47

Fig. 4 Comparison between final configurations of (a) 30 nm long halloysite sheet using the Ewald summation scheme and (b) 90 nm long halloysite sheet using the 8 Å cut-off potential. In both cases the simulation temperature equals 250 K.
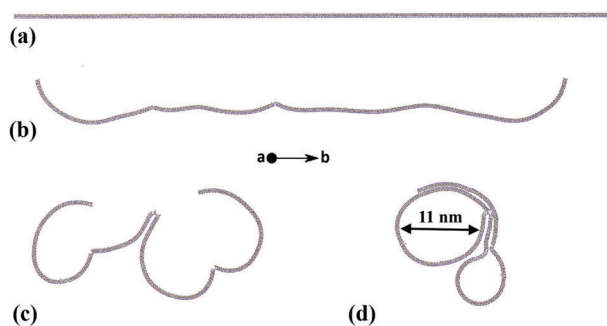

Fig. 5 Time evolution of the 90 nm long halloysite sheet rolled around the *a* axis and obtained by using the Ewald summation scheme at (a) 0 ns, (b) 1 ns, (c) 2 ns and (d) 3 ns. Simulation temperature equals 250 K.

Next, we calculated the dynamics of the 90 nm halloysite sheet using Ewald summation (Fig. 5). Periodical boundary conditions were applied along all directions with 400 Å of vacuum added to the *b* and *c* directions from both sides. The resulting configuration is of the twin-tubular form, with an inner diameter of around 11 and 6 nm, which, as we will show later, agrees with the results obtained with the cut-off potential. The obtained interlayer distance of 7.5 Å is in agreement with the experimental data. This calculation was already very computationally demanding, so for larger systems, we used the cut-off potential.

3.2 Cut-off Coulomb potential scheme

It is known from the literature that the formation of halloysite is mainly related to the rolling process around the *b*-axis, but rolling around the *a*-axis is also possible. In our study, we consider both scenarios. We used a supercell containing 17 000 atoms in total. It was made by replicating the unit cell (34 atoms) along the *a* axis (or *b* axis) and by applying the periodic boundary conditions along the *b* axis (or *a* axis), as visualized in Fig. 3. The atomic positions in the unit cell were initially relaxed by using the first-principles density functional theory method. They are presented in the Appendix.

As the first step of our investigation, we studied the behavior of the kaolinite sheet at very low temperatures. Fig. 6b shows the equilibrium configuration obtained from an isolated kaolinite sheet with the length of 260 nm (Fig. 6a) at 1 K. There is a partial
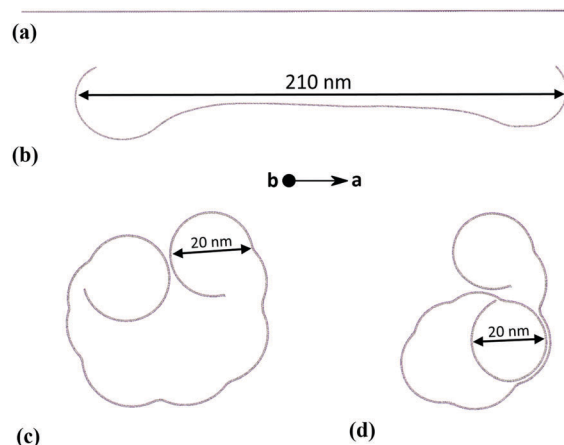

Fig. 6 Transformation of the single kaolin alumosilicate sheet (side view) at different temperatures, using the 8 Å cut-off potential. The length of the unrolled supercell (a) equals 260 nm. The low-temperature configuration (b) was obtained at 1 K. The high-temperature (250 K) structures were visualized at 10 ns (c) and 25 ns (d). The calculated energy of the resulting structure (d) is equal to −5210 eV (per unit cell).

rolling of the supercell ends, and at the same time, the central part remains almost flat. We found that the rolling process can be further stimulated by increasing the temperature from 1 K to 250 K. Fig. 6 gives the intermediate (c) and equilibrium (d) structures at 250 K. The resulting structure is complex and contains a single-walled tube with a diameter of 20 nm in the inner part. Similar results were obtained for the temperature range from 200 K to 300 K.

The molecular dynamics simulations discussed above were performed with the periodical boundary conditions in the *a* direction. In this case, the kaolinite sheet was forced to roll around the *b* axis. If we apply the periodical boundary conditions along the *b* axis, then the rolling occurs around the *a*-axis, and in this case, the inner diameter of tubular halloysite equals 30 nm (Fig. 7). The calculated inter-layer distance is 13 Å, which is about two times larger than that reported for the halloysite nanotubes
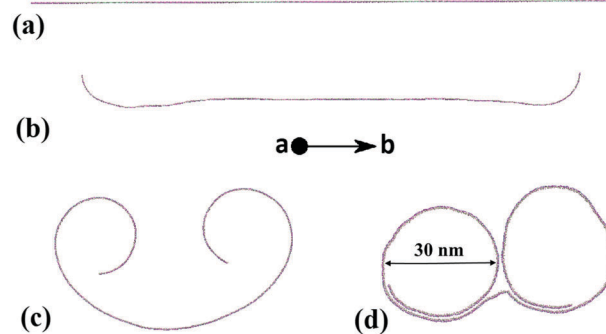

Fig. 7 Time evolution of halloysite rolled around the *a* axis (side view) at different temperatures, using the 8 Å cut-off potential. The length of the unrolled supercell (a) equals 275 nm. The low-temperature configuration (b) was obtained at 1 K. The high-temperature (250 K) structures were visualized at 2.5 ns (c) and 5 ns (d). The calculated energy of the resulting structure is equal to −5450 eV (per unit cell).

with a layer spacing of 7.5 Å (anhydrous form) and close to the halloysite modification with water molecules (hydrous). Remarkably, the evolution of the kaolin alumosilicate sheet to the tubular form around the *a* axis is much faster than that in the case of the *b* axis configuration. The resulting structure presented in Fig. 7d has a distinct twin-tube form. The discussed results are in good qualitative agreement with our Ewald calculations (Fig. 5). The most notable differences are the inner radius and interlayer spacing, which are somewhat larger in the case of the cut-off potential calculations.

In principle, the models we use can be extended to take into account water molecules interacting with halloysite. Numerous experimental studies[25,26] revealed an important role of water in technological applications of clay minerals. From the theoretical side, the previous molecular dynamics study[16] of different slab models of halloysite demonstrated no particular changes in the clay and water molecules. However, a pronounced ordering of the water molecules on the octahedral surface was detected. Thus, it is interesting to understand the effect of the water on the rolling of the kaolinite sheet. We left this for future investigations.

Experimental verification of the theoretical models. To provide an experimental support to the molecular dynamics simulations described above, we performed AFM experiments. Experimentally, imaging of halloysite nanotubes is normally performed using electron microscopy, both scanning and transmission.[27] Although electron microscopy allows for obtaining high resolution images of halloysite, it does not allow the three-dimensional structure of clay nanotubes to be fully reconstituted. Here, we resorted to AFM operated in the PeakForce Tapping nanomechanical imaging mode to obtain topography images and build 3D reconstructions of the clay nanotubes. The PeakForce Tapping AFM imaging mode is a non-resonant AFM method based on the direct force measurement of surface topography with simultaneous force curve capturing at each pixel of the scan.[28] Fig. 8a shows a typical AFM image (PeakForce Tapping topography) of the halloysite nanotubes, the majority of the particles exhibit a typical rod-like morphology. However, a
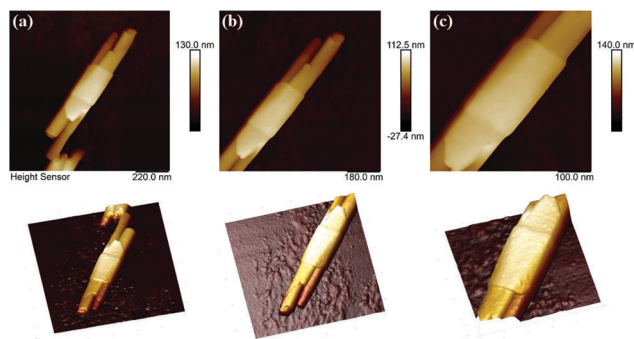
Fig. 9 Double-twisted nanotube (a scroll enclosing two nanotubes). The upper row shows the increasing magnification 2D topography images, the lower row shows the respective 3D topography reconstructions of images (a–c).

careful examination suggests that a single tube (indicated by an arrow) has a distorted conical morphology. We were able to isolate and image several conical tubes (Fig. 8b). These experimentally found morphologies fully support our computational models. We also imaged the spiral ending of a single halloysite nanotube (Fig. 8c). Interestingly, we were able to find a very peculiar defected nanotube (Fig. 9), which apparently demonstrates a morphology predicted theoretically in Fig. 7d. This nanotube represents the case when a single large nanoscroll (having *ca.* 190 nm diameter) engulfs two smaller nanotubes having 70 and 97 nm diameters, respectively. Although the dimensions of this nanotube are larger than those used in our calculations, the overall morphology of the twinned nanotube suggests that similar smaller nanotubes may also exist.

Dependence on length. Such a tendency to form twin-tube structures can also be revealed in simulations of the supercells with lengths of up to 180 nm presented in Fig. 10. One can see that the single-walled nanotube can be formed from the 90 nm kaolin alumosilicate sheet. Importantly, the diameter of the nanotube is about 30 nm, which is within the experimental range.[29] At the same time, the obtained diameter of the single-walled nanotube is about four times larger than that used in the previous theoretical simulations.[4] The 180 nm long kaolin sheet transforms into a twin-tube structure at high temperatures, which is similar to what we observe for the sheet with the length of 275 nm (Fig. 7).

Based on the obtained results of the molecular dynamics simulations, we conclude that the temperature is not the only external parameter that is responsible for the formation of the halloysite nanotube with a spiral multi-walled structure. For that, one needs to consider different types of distortions of the initial kaolinite sheet and the effect of external pressure. We left this for future investigations.

Artificial rolling. The structures (Fig. 6 and 7) obtained from the molecular dynamics simulations differ from ideal nanotubes with the spiral inner structure described in the literature. That is why the next step of our investigation was to simulate the artificially rolled halloysite nanotubes with pre-defined geometry. Previously, such an approach was used in a number
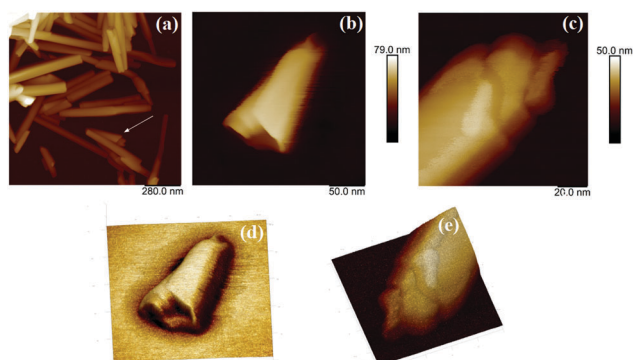
Fig. 8 AFM images of conical nanotubes: (a) a single conical nanotube within a rod-shaped tube sample, (b) a topography image of a single conical tube, (c) a topography image of a spiral tube ending, (d) modulus map superimposed onto the 3D topography image of the tube shown in (b) and (e) a 3D topography image of the tube shown in (c).
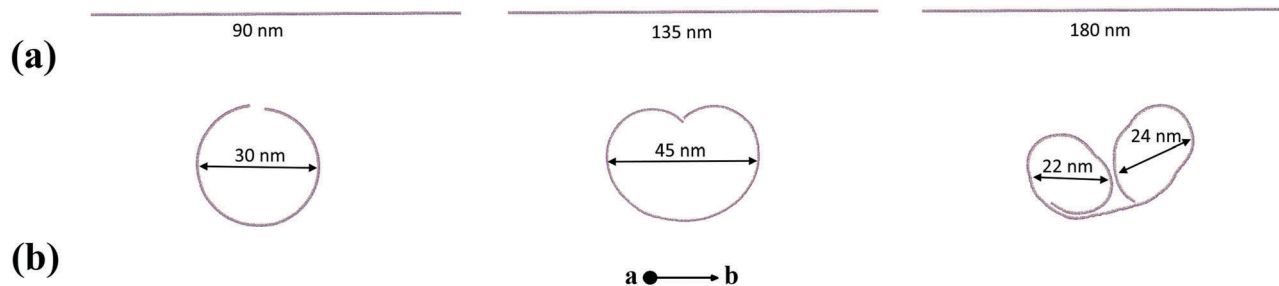
Fig. 10 Time evolution of 90, 135 and 180 nm long kaolin sheets rolled around the *a* axis at 0 ns (a) and 4 ns (b). The simulation temperature equals 250 K.

of theoretical investigations. For instance, the authors of ref. 4 have simulated the electronic and mechanical properties of single-walled halloysite nanotubes with a largest diameter of about 4 nm. A more realistic model with overlapping arms was proposed and studied in ref. 15. However, the diameter of the simulated spiral nanotube of 5 nm was still much smaller than the experimental one.

In order to generate the spiral structures with characteristics close to those experimentally observed, a correspondence must be established between the atomic coordinates in the initial and curved lattices. This is done as follows. Let x, y, and z be the Cartesian coordinates of atoms in the plate slab with thickness h in the ab-plane ($0 \leq z \leq h$). When the slab is bent into a tube with the winding axis parallel to the a-direction, the atomic coordinates are transformed according to the rule

$$x \rightarrow X = x,$$

$$y \rightarrow Y(z, \varphi) = \left(R_{in} + h - z + \frac{\Delta}{2\pi} \varphi \right) \sin \varphi, \qquad (6)$$

$$z \rightarrow Z(z, \varphi) = \left(R_{in} + h - z + \frac{\Delta}{2\pi} \varphi \right) (1 - \cos \varphi),$$

where R_{in} is the inner radius of the spiral and Δ is its pitch. The atoms with $z = h$ are thus placed on the inner side of the spiral and $z = 0$ corresponds to the outer side. The angle φ is obtained from the condition that the arc length of the inner side of the spiral is equal to the length of the corresponding original plate structure: $AB = A'B'$ (see Fig. 11). This leads to the equation

$$y = \int_0^\varphi \sqrt{Y_\phi'^2 + Z_\phi'^2} \, d\phi, \quad z = h, \qquad (7)$$

whence the angle φ can be numerically derived for any atom. Eqn (6) and (7) provide the one-to-one correspondence between the atomic coordinates x, y, z in the planar layer and the coordinates X, Y, Z of atoms in the spiral tube.

We constructed ideal multi-walled a-axis halloysites with different structural parameters (diameter and number of layers). The inter-layer distance in these structures was set to the experimental value of 7.5 Å. These structures were found to be stable during MD simulations. The results of these simulations (Table 2) demonstrate weak dependences of the total energy on the number of layers and diameter, the relative changes are about 1%. Nevertheless, the total energy decreases with increasing diameter
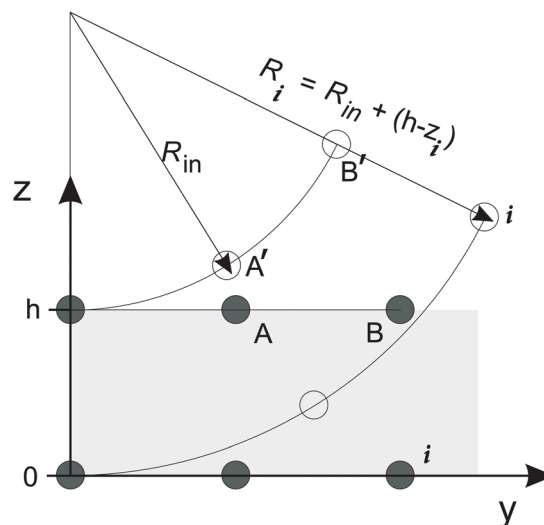

Fig. 11 Model demonstrating transformation of the kaolin sheet to a tubular form.

Table 2 Structural parameters and calculated energies for the different forms of halloysite artificially rolled around the *a* axis. The simulation temperature was chosen to be 250 K

Diameter (nm)	Layers	Energy (eV per cell)
Fixed diameter		
5.0	4	−5241
5.0	1–2	−5297
Fixed sheet length		
5.0	4	−5241
8.0	3–4	−5279
13.0	2–3	−5307
Fixed number of layers		
5.0	1–2	−5297
30.0	1–2	−5333
50.0	1–2	−5364

of the nanotube for the systems rolled from the kaolin sheets of the same length. At high temperatures, the system favors the increasing of the diameter and decreasing of the number of layers (Table 3). We obtain a similar tendency for the halloysite with the winding axis in the b direction. Based on these results, we conclude that the optimal diameter corresponding to the

Table 3 Structural parameters and calculated energies for the different forms of halloysite artificially rolled around the *b* axis. The simulation temperature was chosen to be 250 K

Diameter (nm)	Layers	Energy (eV per cell)
5.0	1–2	−5097
20.0	1–2	−5162
40.0	1–2	−5229

minimum of the total energy of the artificially rolled nanotubes is larger than 50 nm.

Interestingly, the results obtained for the artificial rolled halloysite suggest that rolling around the *a*-axis is more energetically favorable than rolling around the *b*-axis.

For the artificial rolled halloysite models, we calculated the Young's modulus. These values are 91, 117 and 144 GPa for the 3-, 5- and 10-layer models, respectively. The inner diameter of the halloysite nanotubes in these simulations was fixed at 10 nm. The calculated values of the Young's modulus agree with the experimental estimate[30] of 130 ± 24 GPa. However, the theoretical results can change if one takes into account defects that inevitably exist in real-world halloysite nanotubes.

Open boundary conditions. The results discussed above were obtained for the supercells with the periodic boundary conditions applied along the *b* or *a* axis. The low-temperature molecular dynamics evolution of the square sheet of halloysite with open boundary conditions is presented in Fig. 12. The corresponding supercell contains 91 and 55 unit cells along the *a* and *b* axes, respectively. This corresponds to a system with 170 170 atoms in total. One can see that the flat geometry of the square kaolin sheet is unstable even at the very low temperature of 1 K. As a result, a partial rolling of the square sheet takes place. Remarkably, the winding axis is parallel to the *b* axis, which is in agreement with the experimental observations. In the case of high temperature, the final stable configuration is rolled around the diagonal of the square sheet. The resulting diameter of the rolled structure is about 27 nm, which is also in the experimental range.
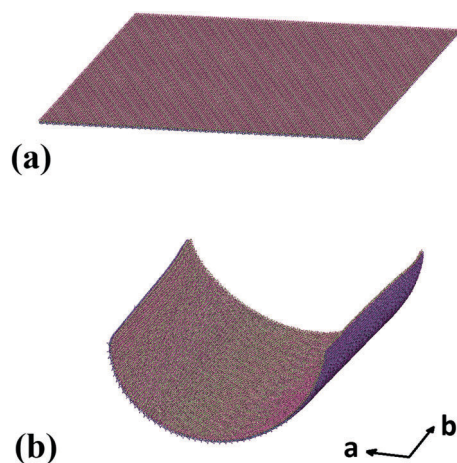

Fig. 12 Low-temperature molecular dynamics evolution of the halloysite square sheet 50 × 50 nm at 0 ns (a) and 5 ns (b).
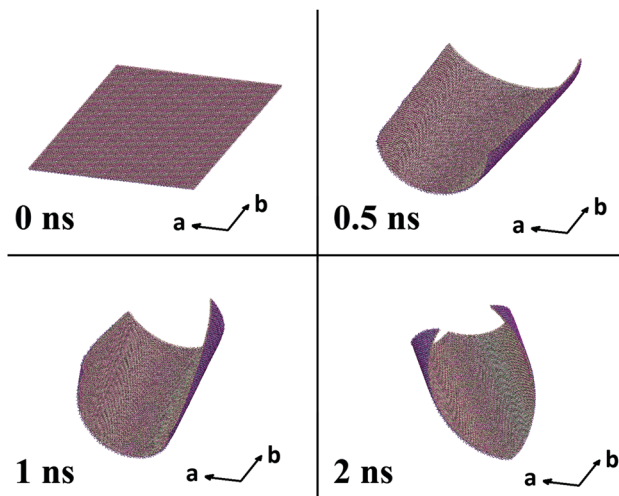

Fig. 13 Molecular dynamics evolution of the halloysite square sheet 50 × 50 nm at 250 K.
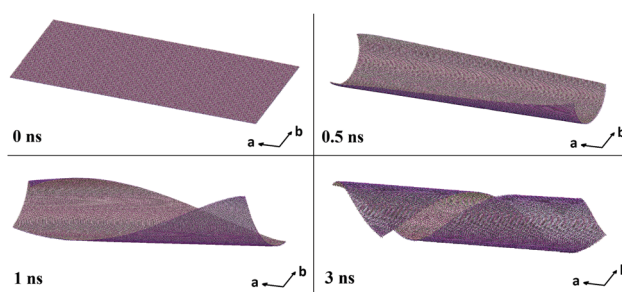

Fig. 14 Molecular dynamics evolution of the halloysite rectangular sheet 145 × 50 nm at 250 K.

The simulations with the rectangular supercells of 145 nm × 50 nm (486 540 atoms in total) elongated in the *a* and *b* directions revealed the formation of twisted structures with a diameter of 27 nm (Fig. 14). This is similar to the case of the carbon nanotubes formed from graphene nanoribbons.[31] Importantly, the molecular dynamics simulations performed in that work[31] have shown that the edges of a twisted nanoribbon come close enough to establish a bonding formation, which acts as an initiator for zipping to proceed towards the rest of the ribbon until a complete tube is formed. In our case, we do not expect such an edge bonding since it requires oxygen vacancies to be introduced in the system under consideration.

Change of the inter-atomic distances. As was mentioned in the introduction, the main reason for the halloysite rolling is believed to be the difference in lengths of the Al-dioctahedral and Si-tetrahedral sheets. To show a numerical comparison between the different resulting structures, we calculated average bond lengths for Al–O octahedra and Si–O tetrahedra. From Table 4, we can see that with respect to a single kaolinite sheet, the size of the Si–O tetrahedra stays the same, while the size of the Al–O octahedra decreases. The tube rolled around the *b*-axis demonstrates the biggest reduction in Al–O octahedra size, which also results in the lowest inner tube diameter. On the

Table 4 Calculated average bond length for Al–O octahedra, Si–O tetrahedra and distance between layers inside the halloysite tube

Structure	Al–O (Å)	Si–O (Å)	Interlayer distance (Å)
Fig. 2	2.07	1.60	—
Fig. 6d	2.01	1.60	12.0
Fig. 7d	2.04	1.60	13.0
Fig. 13 (2 ns)	2.02	1.60	—

contrary, the tube rolled around the *a*-axis demonstrates the smallest reduction in Al–O octahedra size. This can be attributed to the atomic structure of the halloysite, where the *a*-axis direction is corresponding to the zig-zag direction and the *b*-axis is corresponding to the armchair direction of Al and Si hexagons.

The interlayer distances provided in Table 4 correspond to the distance between identical atoms in neighboring layers. Those interlayer distances are somewhat larger than the experimental one, which is 7.5 Å. This can be explained by the lack of non-bonded interaction between hydroxyl H and bridging O in the potential that we used.

4 Conclusion

In this work, we studied the dynamics of halloysite rolling without water under different conditions. Using a well-established inter-atomic potential for clay materials, we have demonstrated that a partial rolling of the kaolin sheet can already occur at low temperatures. At ambient temperatures, halloysite rolls and forms complex tubular structures with inner diameters of about 10–30 nm. We demonstrated that rolling occurs around both the *a* and *b* crystallographic directions. However, a large difference between the rates of the rolling process for different directions is observed. We showed that the exclusion of long-ranged contributions from the Coulomb energy increases inner diameter and interlayer distance, but overall, dynamics stay qualitatively the same. The theoretically predicted formation of the twin-tube profiles of the halloysite was confirmed by our AFM experiments. The simulations for the models with open boundary conditions demonstrated formation of twisted geometries, which is similar to the case of graphene nanoribbons. Our study opens a way for the realistic simulation of halloysite contacting with different molecular complexes, metallic nanoparticles and other systems of technological importance.

Conflicts of interest

There are no conflicts to declare.

Appendix

Table 5 contains the optimized atomic positions obtained from the first-principles density-functional theory calculations.

Table 5 Cartesian atomic coordinates for halloysite unit cell adopted in this work

x (Å)	y (Å)	z (Å)
a, b, c unit cell vectors		
5.153	0	0
0.032	8.942	0
1.918	−0.242	7.133
Al in octahedral coordination		
0.489	6.721	3.317
0.456	3.791	3.324
3.050	2.291	3.317
3.049	8.262	3.324
Si in tetrahedral coordination		
4.876	5.400	0.669
2.283	0.929	0.669
2.218	6.948	0.646
4.779	2.477	0.646
O in octahedral sheet		
1.461	2.519	4.344
4.053	6.990	4.344
1.484	8.014	4.313
4.044	3.543	4.313
1.072	5.270	4.330
3.633	0.799	4.330
2.071	3.596	2.318
4.664	8.067	2.318
Si in Si–O–Si coordination		
3.444	1.825	0.007
0.883	6.296	0.007
3.439	5.976	0.214
0.846	1.505	0.214
2.422	8.405	0
5.015	3.845	0
2.398	0.816	2.274
4.990	5.287	2.274
2.094	6.971	2.260
4.655	2.500	2.260
H in clay mineral hydroxyl groups		
3.803	6.579	5.193
1.211	2.108	5.193
1.203	8.279	5.221
3.796	3.808	5.221
1.350	5.220	5.271
3.911	0.749	5.271
2.562	4.438	2.325
5.123	8.908	2.325

Acknowledgements

References

1 E. Joussein, S. Petit, J. Churchman, B. Theng, D. Righi and B. Delvaux, *Clay Miner.*, 2005, **40**, 383–412.

2 Y. Lvov, W. Wang, L. Zhang and R. Fakhrullin, *Adv. Mater.*, 2016, **28**, 1227–1250.

3 M. Liu, Z. Jia, D. Jia and C. Zhou, *Prog. Polym. Sci.*, 2014, **39**, 1498.

4 L. Guimaraes, A. N. Enyashin, G. Seifert and H. A. Duarte, *J. Phys. Chem. C*, 2010, **114**, 11358–11363.

5 B. Singn, *Clays Clay Miner.*, 1996, **44**, 191–196.

6 B. Singn and I. Mackinnon, *Clays Clay Miner.*, 1996, **44**, 825–834.

7 K. Tazaki, *Clays Clay Miner.*, 2005, **53**, 224.

8 J. Kirkman, *Clays Clay Miner.*, 1981, **29**, 1.

9 Y. Kuroda, K. Ito, K. Itabashi and K. Kuroda, *Langmuir*, 2011, **27**, 2028.

10 I. D. M. Robertson and R. A. Eggleton, *Clays Clay Miner.*, 1991, **39**, 113–126.

11 B. Singn and R. Gilkes, *Clays Clay Miner.*, 1992, **40**, 212–229.

12 N. Kohyama, K. Fukushima and A. Fukami, *Clays Clay Miner.*, 1978, **26**, 25–40.

13 R. Anand, R. Gilkes, T. Armitage and J. Hillyer, *Clays Clay Miner.*, 1985, **33**, 31–43.

14 S. W. Bailey, Surface Chemistry Structure and Mixed Layering of Clays. Proceedings of the 9th Int. Clay Conf. Sciences Geologiques, Memoire, 8**6**, Strasbourg, France, 1990, 89–98.

15 F. Ferrante, N. Armata and G. Lazzara, *J. Phys. Chem. C*, 2015, **119**, 16700–16707.

16 D. Presti, A. Pedone, G. Mancini, C. Duce, M. R. Tine and V. Barone, *Phys. Chem. Chem. Phys.*, 2016, **18**, 2164–2174.

17 K. Momma and F. Izumi, *J. Appl. Crystallogr.*, 2008, **41**, 653–658.

18 G. Fakhrullina, F. Akhatova, M. Kibardina, D. Fokin and R. Fakhrullin, *Nanomedicine*, 2017, **13**, 483–491.

19 S. Plimpton, *J. Comput. Phys.*, 1995, **117**, 1–19.

20 R. T. Cygan, J.-J. Liang and A. G. Kalinichev, *J. Phys. Chem. B*, 2004, **108**, 1255–1266.

21 D. L. Bish, *Clays Clay Miner.*, 1993, **41**, 738–744.

22 G. Kresse and J. Furthmüller, *Phys. Rev. B: Condens. Matter Mater. Phys.*, 1996, **54**, 11169.

23 G. Kresse and D. Joubert, *Phys. Rev. B: Condens. Matter Mater. Phys.*, 1999, **59**, 1758–1775.

24 J. Perram, H. G. Petersen and S. de Leeuw, *Mol. Phys.*, 1998, **65**, 875–893.

25 H. N. Bordallo, L. P. Aldridge and A. Desmedt, *J. Phys. Chem. B*, 2006, **110**, 17966–17976.

26 H. N. Bordallo, L. P. Aldridge, G. J. Churchman, W. P. Gates, M. T. F. Telling, K. Kiefer, P. Fouquet, T. Seydel and S. A. J. Kimber, *J. Phys. Chem. C*, 2008, **112**, 13982–13991.

27 Y. Lvov, M. DeVilliers and R. Fakhrullin, *Expert Opin. Drug Delivery*, 2016, **13**, 977–986.

28 G. Smolyakov, C. Formosa-Dague, C. Severac, R. E. Duval and E. Dague, *Micron*, 2016, **85**, 8–14.

29 K. A. Zahidah, S. Kakooei, M. C. Ismail and P. B. Raja, *Prog. Org. Coat.*, 2017, **111**, 175–185.

30 D. Lu, H. Chen, J. Wu and C. M. Chan, *J. Nanosci. Nanotechnol.*, 2011, **11**, 7789–7793.

31 H. E. Lim, Y. Miyata, R. Kitaura, Y. Nishimura, Y. Nishimoto, S. Irle, J. H. Warner, H. Kataura and H. Shinohara, *Nat. Commun.*, 2013, **4**, 2548.

32 V. Voevodin, S. Zhumatiy, S. Sobolev, A. Antonov, P. Bryzgalov, D. Nikitenko and K. Stefanov, *Open Syst. J.*, 2012, **7**, 36–39.